Raman analysis of oxide cladded Silicon core nanowires grown with solid silicon feed stock

*Parul Sharma, V. Stolojan and S. R. P. Silva**

Nano-Electronics Centre, Advanced Technology Institute, University of Surrey, Guildford, UK GU2 7XH

*s.silva@surrey.ac.uk

INTRODUCTION

One-dimensional nanostructures have attracted much attention due to their novel properties and potential applications in nanoelectronics and nanophotonics (Tian et al. 2007; Byun et al. 2009; Chan et al. 2008). Over the past decade, silicon nanowires have been synthesized and studied for their nanoscale properties Li et al. 2005; Kim et al. 2009). Structures of nanoscale dimensions show enhancement of properties, most often independent of the material system Guo et al. 2008; Bhattacharyya et al. 2006). Oxide clad can increase thermal stability of nanowire by protecting the crystalline silicon core from further oxidation. Oxide clad has shown its application in fabricating surround-gate field effect transistors (Ng et al. 2004). In developing silicon nanowires with oxide clad, for large scale applications, it is important to develop simple, reproducible and controllable growth strategies for obtaining crystalline silicon nanowires with large aspect ratios, typically greater than 1000. VLS (Zhao et al. 2008; Kawashima et al. 2008) growth with silane as a silicon source and Au as a catalyst is a well known method to synthesize crystalline silicon nanowires with large aspect ratios. Other methods, such as pulsed laser deposition (PLD) (Morales et al. 1998), metal organic vapor phase epitaxy (MOVPE) (Hiruma et al. 1993) and chemical beam

epitaxy (CBE) (Ohlsson et al. 2001) are employed to grow silicon nanowires. These methods require complicated experimental setups, with increased costs. We present the synthesis of silicon nanowires by combining a SLS mechanism with a VLS mechanism in this paper. This method does not need a complicated experimental setup or the use of the hazardous gas silane. It is a growth method which is cost-effective, large-area-compatible and may give a higher degree of control of the end product, facilitated by the simple experimental process. In the VLS mechanism, a gold-coated silicon wafer is used as a substrate and a Si precursor is thermally degraded from the gas phase over the substrate whilst the Au film breaks up into islands. The Si from the precursor dissolves into the gold droplets to form eutectic gold silicide, until saturation. Upon saturation, Si extrudes from the droplets as nanowires. In the SLS mechanism (Lee et al. 2004; Lee et al. 2008), the Si wafer itself acts as a silicon source in the growth and Si nanowires grow by thermal annealing, assisted by the transition metal coating on the silicon wafer. These mechanisms have the advantage of controlling the nanowire diameter through the size of the nucleating metal island. Our synthesis method combines the SLS mechanism for the initial formation of metal islands (Au or Ni), their saturation with Si and the extrusion of nanowire growth, which is then sustained via a VLS mechanism (Sharma et al. 2010). The SiNWs are also interesting from the fundamental point of view due to the changes in the basic electronic and vibrational properties with respect to the bulk. Several researchers have observed phonon confinement effects in semiconductor nanowires using Raman spectroscopy. Raman spectroscopy is a non-destructive, simple to use and fast method to study nanowires. It provides information with regard to the surface and volume phonon modes and lattice vibrations, including how those vibrations are affected by extreme small dimensions. We have used Raman spectroscopy to analyze and compare the grown silicon nanowires when using gold or nickel as the catalyst.

EXPERIMENTAL SECTION

SiNWs were grown at 1000^{o}C in tube furnace through thermal annealing. The samples used in the experiment are Au/Si and Ni/Ti/Si with thicknesses of 20nm Au, 20nm Ni and 100nm Ti. Au, Ni and Ti were deposited using a DC-magnetron sputtering system from JLS, using Ar at a pressure of 5mTorr with 25sccm flow rate. The substrate was <100> single crystalline Si. Si nanowires were synthesized by the following method: the sample was placed into a quartz tube in a tube furnace which was then heated to 1000^{o}C in two steps: firstly, for one hour in vacuum and

secondly under a flow of H_2, at a rate of 80sccm for an hour, while maintaining the pressure at 250mbar. Then the furnace was allowed to cool to room temperature under a constant flow of He, for 3 hours at 100sccm.

RESULTS & DISCUSSION

A FEI Quanta 200 Scanning electron microscope (SEM) was used to image the nanowires. The structure and composition was studied using energy-filtered transmission electron microscopy (EFTEM, Philips CM200ST 200keV, LaB6 source, fitted with a Gatan Imaging Filter). The optical properties were analyzed using micro Raman spectroscopy (Reinshaw 2000), with a diode laser as the excitation source (782nm, 1mW). The nanowires were detached from their Si substrate onto the glass surface for Raman analysis. The glass surface showed no Raman features in the region of interest ($100cm^{-1}$ to $600cm^{-1}$).

The SEM images shown in Fig1 (a and b) show high densities of SiNWs. SiNW in the samples A and B were synthesized with Ni/Ti and Au metal catalysts respectively. The average core-diameters for the two samples are similar, of the order of 10nm. However, the nanowires grow to lengths of about ~ 1µm in sample Ni/Ti (Fig1a) and significantly longer, of up to tens of µm in sample Au (Fig1b); the actual length was difficult to measure due to entanglement of the nanowires.

The elemental distribution within SiNWs in sample A and sample B was mapped using EFTEM. Highresolution imaging and diffractograms show that the grown nanowires have core-clad structures, with a crystalline core cladded by an amorphous coating. Fig3(a) shows the elemental distribution for SiNWs grown on sample A, revealing a Ni and Si mix at the catalyst tip, most likely as a silicide. SiNWs in sample A have a crystalline Si core covered with an amorphous oxide clad (Fig3b). The oxide clad is much thicker than the native oxide thickness (~2-5nm) which forms by oxidation of silicon nanowires in ambient air, as is the case where nanowires are grown with silane via CVD. The average diameter (15.5nm) of the crystalline core is determined from the HRTEM micrographs of 100 SiNWs in sample A. The corresponding size distribution is given in Fig4(a). Fig4(b) shows a linear relationship between the core diameter and the total wire diameter, with a slope of 0.45±0.5nm.

$$\frac{D_{core}}{D_{total}} = (0.45 \pm 0.5) nm \qquad (1)$$

Where D_{core} is the core diameter and D_{total} is the total nanowire diameter. This constant ratio suggests that the oxide clad and the Si core is formed during the same process and is controlled purely through the catalyst size. (Fig3c). The presence of the catalyst particle on the tip and the constant diameter of the wires indicate that these nanowires grow via a VLS mechanism, where a steady state between Si arriving at the catalyst and Si being extruded from the catalyst is achieved. The straight line fit in Fig4b also shows that no nanowires are obtained below 24.5nm. This can be interpreted as the critical catalyst size below which it is not forming a nanowire. The critical catalyst size manifests the thermodynamic limit for the minimum radius of the catalyst droplets.

The Raman spectra for sample A and sample B are shown in Fig2a and Fig2b respectively. To reduce the effect of laser heating on the Raman spectrum, a low intensity laser power of 1mW was used to analyze our samples. Detailed information on the effects of laser heating on features of the Raman spectra of Si nanowires grown with Ti and Ni seedbed structure has been discussed elsewhere (Sharma et al. 2010; Anguita et al. 2009). We will concentrate on the changes in the first-order optical mode, when compared to standard c-Si. A Raman peak at 521.1cm^{-1}, with the full-width-at-half-maximum of 4.1cm^{-1} was observed for c-Si. This is due to the scattering of the first-order optical phonon of c-Si. The Raman spectra of samples A and B (in Fig2a and Fig2b) show prominent Raman features at ~515.4 and ~513.4cm^{-1}, respectively, with a shoulder at 495.2 and 490.6cm^{-1}, respectively. In addition, there are two broad peaks at ~950 and 290cm^{-1}. When comparing them with the c-Si Raman spectrum, SiNWs on samples A and B show a similar band, exhibiting broader widths and a red shift in the peak positions. Note that the nanowires no longer lie on the crystalline silicon substrate, but have been transferred onto glass. This feature has also been observed by other research groups for crystalline silicon nanowires (Chen et al. 2007,Pan et al. 2005). The observed line width broadening can be explained with the breakdown of the phonon momentum selection rule q≈0, specific of the Raman scattering in ordered systems. In the case of crystals of very small size, this rule is no longer valid as the phonons are confined in space and all the phonons over the Brillouin zone will contribute to the first order Raman spectra. The weight of the off-center phonon increases as the crystal size decreases and the phonon dispersion causes an asymmetrical broadening and the shift of the Raman peaks (Campbell et al. 1986; Bersani et al. 1998). Spectral parameters of the first-order optical phonon spectra of SiNWs (sample A and B) and of c-Si are listed in Table 1. The spectral parameters are the Raman frequency, the frequency shift, the coefficient of broadening (C_b) defined by $FWHM_{SiNWs}/FWHM_{c\text{-}Si}$, and the asymmetric coefficient (C_a)

defined by LWHM/RWHM, where LWHM and RWHM are the left-width-at-half-maximum and right-width-at-half-maximum from the central peak position respectively. From Table 1, we found that the frequency shift, FWHM, the coefficient of broadening C_b, and the asymmetric coefficient C_a of sample B are all larger than those of sample A. This is expected qualitatively from the values in the order of size measured by TEM listed in Table 1, giving further support to that the Raman spectra shown in Fig2a and 2b result from the quantum confinement effect of the SiNW samples A and B.

The phonon confinement model has been widely used to study the low dimensional effect on the phonon Raman spectra. According to theoretical calculations based on the phonon confinement model of Richter et. al. (Richter et al. 1981) and Campbell and Fauchet (Campbell et al. 1986), the Raman intensity of particles of diameter L is expressed as shown in the following equation

$$I_0(\omega) \sim \int \frac{|C(0,q)|^2}{[\omega - \omega(q)]^2 + \left(\frac{\Gamma_0}{2}\right)^2} d^3q, \quad (2)$$

Where C(0,q) is a Fourier coefficient of the confinement function, ω(q) is the phonon dispersion function and Γ0 is the full-width-at-half-maximum for the bulk material, which in our experimental conditions is 4.1cm^{-1}. q is the phonon wave vector, which is expressed in units of 2π/a, where a is the lattice constant of silicon. Considering the basic shape and material of our nanowire samples, we have used

$$|C(0,q)|^2 = exp\left(\frac{q^2L^2}{16\pi^2}\right), \quad (3)$$

and

$$\omega(q) = \left[A + B\cos\frac{qa}{2}\right]^{0.5}, \quad (4)$$

with A=1.714×105cm-2, B=1×105cm-2. The integration is performed over the entire Brillouin zone. This intensity function was fitted to our experimental data and the comparison between the experiment and the simulation based on the phonon confinement model is shown in Fig2a and Fig2b for samples A and B respectively. The Raman peak variation with nanowire diameter has been shown in Fig4 (c and d), measured by equation 1 with different L values. Straight line at 515.4cm^{-1} and 513.4cm^{-1} in Fig4c and Fig4d is Raman peak for SiNWs grown with Ni and Au

catalyst respectively. Error bars of ±2cm^{-1} are shown in curves for both SiNW peaks. Nanowire diameters for sample A and sample B by Raman fitting provides 11.5±3.5nm and 9.5±2nm, as their diameters as listed in table 1. There is good general agreement in spectral features between experimental and calculated Raman spectra, indicating that the identification of the Raman peak at ~513.4 and ~515.4cm^{-1} in figures 4a and 4b is correct.

On closer examination, some discrepancies have been observed between the experimental and the calculated spectra. The calculated spectra do not explain the features on the low frequency sides with shoulders at ~490.6cm^{-1} for sample A and ~495.2cm^{-1} for sample B, suggesting that there are other components not due to the SiNWs. They may be attributed (Veprek et al. 1987) to the oxide that covers the SiNWs, which has a Raman structure between 400cm^{-1} and 550cm^{-1}, with a peak at ~490cm^{-1}.

Growth conditions have been investigated with more experiments. Critical growth temperatures were examined by changing the growth temperature. No growth was observed at 950^{o}C, indicating 1000^{o}C is essential for the growth. To investigate the importance of gas in the growth, experiments were carried out without any flow of gas in step two. No nanowire growth was observed on the substrate. SiNW growth with the help of Ti and Ni seedbed structure has been published (Sharma et al. 2010). Growth mechanisms were described with SLS and VLS. In the SLS mechanism, growth temperatures for nanowires depend on the eutectic temperature of the metal silicide, in the present case, no growth was observed at 950^{o}C with Au catalyst also. It should be noted that 950^{o}C is much higher than the eutectic temperature of Au-Si (360^{o}C), indicating the likelihood of another growth mechanism. We suggest a combination of SLS and VLS mechanism to explain the growth in our system. In an initial stage of the growth SLS mechanism start the process, nickel (or Au in sample B) silicide islands form. SiO vapour evaporates from the substrate as a result of the heating Si at 1000^{o}C (Tromp et al. 1995) according to the reaction:

$$Si(s) + SiO_2(s) \rightarrow 2SiO(g)$$

SiO vapour condenses and decomposes at the catalyst head by the action of the catalyst according to the reverse equation:

$$2SiO(g) \rightarrow Si(s) + SiO_2(s)$$

resulting in the formation of solid forms of silicon and silicon dioxide. The temperature is high enough for the decomposition of SiO vapour. A similar observation has been shown in the work of Sharma et. al. (Sharma et al. 2010) where silicon-based nanowires have been grown by the decomposition of SiO at 1000^{o}C. Ping Wu et. al. (Wu

et al. 2007) also reported the vaporization of silicon-containing oxides (SiO_x where $x<2$) at 1000^{o}C and accounted for this process by the mechanism of Si transport in their silica nanowires. After decomposition, the silicon is absorbed into the catalyst island while oxide remains at the surface of the island. Then SiNW grows according to the VLS mechanism. Detailed study for the Ni/Ti/Si substrates with similar growth mechanism can be found in Sharma et. al.(Sharma et al. 2010). They have studied silicon based nanowire growth at 1000^{o}C by combining both the SLS and VLS mechanisms and observed the role of each layer on the growth. A similar dependency on carbon films and CNT growth in the presence and absence of H2 in feedstock hydrocarbon gas was studied by Franceschni et. al. (Franceschni et al. 1986) and F. Ohashi et. al. (Ohashi et al. 2008). Franceschni et. al. (Franceschni et al. 1986) found a strong effect of nitrogen incorporation, from nitrogen precursor gases, on the chemical composition of carbon and nitrogen in the a-C(N)-H film. Similarly, Ohashi et. al. (Ohashi et al. 2008) has studied the role of hydrogen for carbon nanotubes and nanofiber growth. They have changed the morphology of carbon nanofibers grown into nanotubes by changing the hydrogen concentration in the initial reaction stage. Increasing the hydrogen concentration increases the yield but results in more nanofibers.

In summary, we report a novel method for the large scale synthesis of core-clad silicon nanowires by combining the SLS and VLS growth mechanism. Two catalysts (Au and Ni) have been used in the experiment and both samples provide crystalline SiNW growth with this mechanism. Metal islands serve as a starting point of the growth as well as facilitate the SiO formation which further decomposes and nanowire growth takes place. The presence of the catalyst head at the tip from TEM images suggests the growth occurs via a VLS mechanism. HRTEM images show the crystalline Si core covered with oxide of the nanowire. A detailed Raman analysis has been conducted for both samples. Raman peaks of SiNWs have been observed and identified. The spectral features for both samples have been analyzed. A detail calculation based on a phonon confinement model has been performed to interpret the first order Raman-spectra. The diameter of the nanowires has been calculated with this model. There is a discrepancy between the calculated and experimental data. Some reasons for this discrepancy are discussed. Due to the simplicity of the method, it could be adapted in industry for large scale synthesis of silicon nanowires with oxide clad for device fabrication e.g. surround-gate field effect transistors.

ACKNOWLEDGMENT We would like to acknowledge EPSRC Portfolio Partnership Award for sponsoring this work.

REFERENCES

Tian B, Zheng X, Kempa TJ, Fang Y, Yu Y, Yu G, Huang J, Lieber CM (2007) Coaxial silicon nanowires as solar cells and nanoelectronic power sources. Nature 449: 885-889

Byun KE, Heo K, Shim S, Choi HJ, Hong S, Functionalization of Silicon Nanowires with Actomyosin Motor Protein for Bioinspired Nanomechanical Applications (2009) Small 5: 2659-2664

Chan CK, Peng H, Liu G, McIlwrath K, Zhang XF, Huggins RA, Cui Y (2008) High-performance lithium battery anodes using silicon nanowires. Nat. Nanotechnology 3: 31 - 35

Li WN, Ding YS, Yuan J, Gomez S, Suib SL, Galasso FS, DiCarlo JF (2005) Synthesis and characterization of silicon nanowires on mesophase carbon microbead substrates by chemical vapor deposition. J. Phys. Chem. B 109: 3291-3297

Kim DR, Lee CH, Zheng X (2009) Probing Flow Velocity with Silicon Nanowire Sensors. Nano Lett. 9: 1984–1988

Guo XJ, Silva SRP (2008) Science Engineering - High-performance transistors by design. Science 320: 618-619

Bhattacharyya S, Henley SJ, Mendoza E, Rozas LG, Allam J, Silva SRP (2006) Resonant tunnelling and fast switching in amorphous-carbon quantum-well structures. Nat. Mat. 5: 19-22

Ng HT, Han J, Yamada T, Nguyen P, Chen YP, Meyyappan M (2004) Single Crystal Nanowire Vertical Surround-Gate Field-Effect Transistor. Nano Lett. 4: 1247–1252

Zhao H, Zhou S, Hasanali Z and Wang D (2008) J. Phys. Chem. C 112: 5695-5698

Kawashima T, Mizutani T, Masuda H, Saitou T, Fujii M (2008) J. Phys. Chem. C 112: 17121

Morales AM, Lieber CM (1998) A Laser Ablation Method for the Synthesis of Crystalline Semiconductor Nanowires. *Science* 279: 208-211

Hiruma K, Yazawa M, Haraguchi K, Ogawa K, Katsuyama T, Koguchi M, Kakibayashi H (1993) GaAs free-standing quantum-size wires. J. of App. Phys. 74: 3162-3171

Ohlsson BJ, Bjork MT, Magnussun MH, Deppert K, Samuelson L, Wallenberg LR (2001) Size-, shape-, and position-controlled GaAs nano-whiskers. *App. Phys. Lett.* 79: 3335-3337

Lee KH, Yanga HS, Baika KH, Banga J, Vqanfleetb RR, Sigmunda W (2004) Direct growth of amorphous silica nanowires by solid state transformation of SiO_2 films. Chem. Phys. Lett. 383: 380-384

Lee E K, Choi BL, Park YD, Kuk Y, kwon SY, Kim HJ (2008) Nanotechnology 19: 185701-185705

Sharma P, Anguita JV, Stolojan V, Henley SJ, Silva SRP (2010) The growth of silica and silica-clad nanowires using a solid-state reaction mechanism on Ti, Ni and SiO_2 layers. Nanotechnology 21: 295603 (9pp)

Anguita JV, Sharma P, Henley SJ, Silva SRP (2009) Room temperature photoluminescence in the visible range from silicon nanowires grown by a solid-state reaction. IOP Conf. Series: Mat. Sci. and Eng. 6: 012011

Chen Y, Peng B, Wang B (2007) Raman spectra and temperature-dependent raman scattering of silicon nanowires. J. Phys. Chem. C 111: 5855-5858

Pan H, Lim S, Poh C, Sun H, Wu X, Feng Y, Lin J (2005) Growth of Si nanowires by thermal evaporation. Nanotechnology 16: 417–421

Campbell, I. H. Fauchet, P. M. The effects of microcrystal size and shape on the phonon Raman spectra of cristalline semiconductors. *Solid State Commun.* **1986**, 58, 739-741

Bersani D, Lottici PP, Ding XZ (1998) Phonon confinement effects in the Raman scattering by TiO2 nanocrystals. App. Phys. Lett. 72 (1): 73-75

Richter H, Wang ZP, Ley L (1981) The one phonon Raman-spectrum in microcrystalline silicon. Solid State Commun. 39: 625-629

Veprek S, Sarott FA, Iqbal Z (1987) Effect of grain boundaries on the Raman spectra, optical absorption, and elastic light scattering in nanometer-sized crystalline silicon. Phys. Rev. B 36: 3344-3350

Tromp R, Rubloff GW, Balk P, Legoues FK (1985) High-Temperature SiO2 Decomposition at the SiO2/Si Interface**.** Phys. Rev. Lett. 55: 2332-2337

Wu P, Zou X, Chi L, Li Q, Xiao T (2007) Growth model of lantern-like amorphous silicon oxide nanowires. Nanotechnology 18: 125601 (6pp)

Franceschini DF, Freire Jr. FL, Silva SRP (1996) Influence of precursor gases on the structure of plasma deposited amorphous hydrogenated carbon-nitrogen films. App. Phys. Lett. 68: 2645-2647

Ohashi F, Chen GY, Stolojan V, Silva SRP (2008) The role of the gas species on the formation of carbon nanotubes during thermal chemical vapour deposition. Nanotechnology 19: 445605

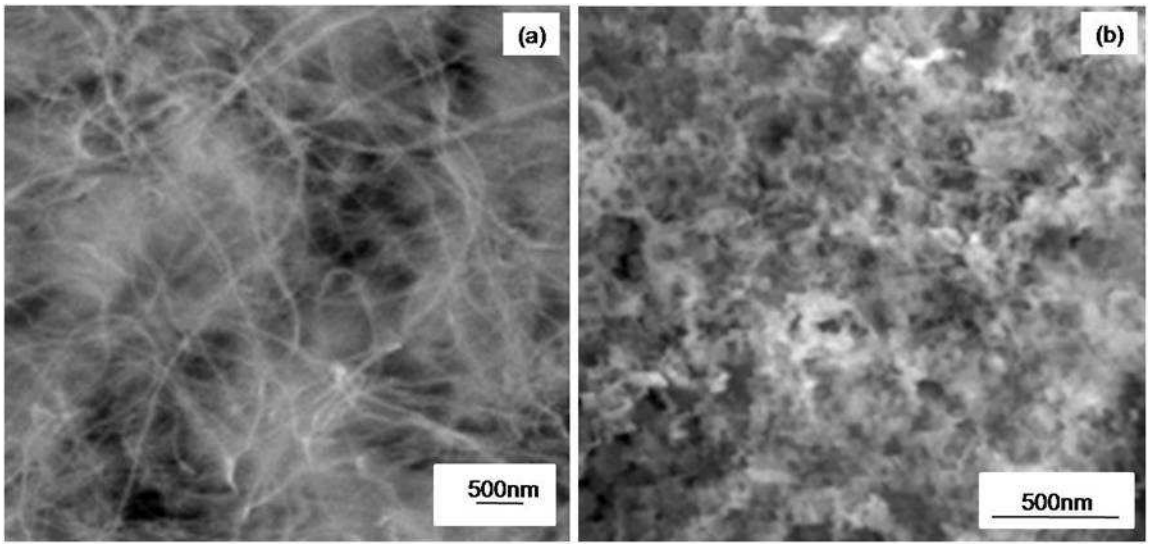

Fig.1 Core-clad Si nanowires growth with (a) Ni/Ti/Si substrate (sample A) and (b) Au/Si substrate (sample B). The scale is 500nm for both images.

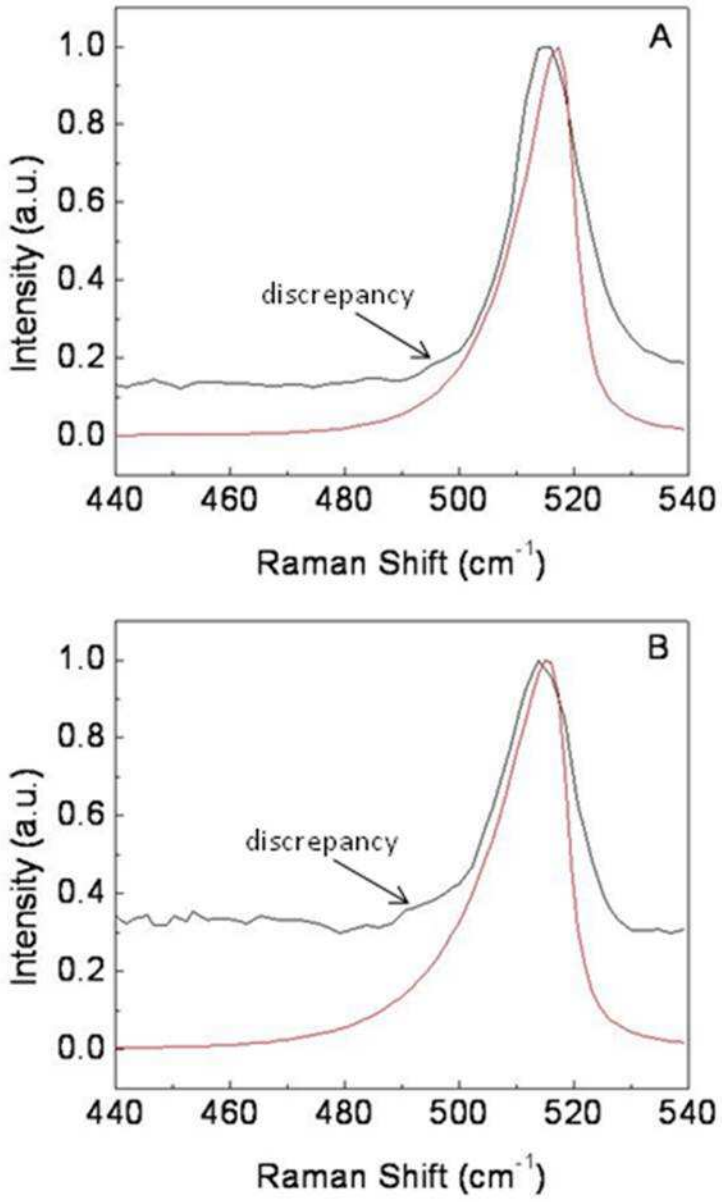

Fig.2 Measured (black line) and calculated (red line) first order Raman spectra (a) for SiNWs grown on Ni/Ti/Si substrate (sample A) and (b) SiNWs grown on Au/Si substrate (sample B).

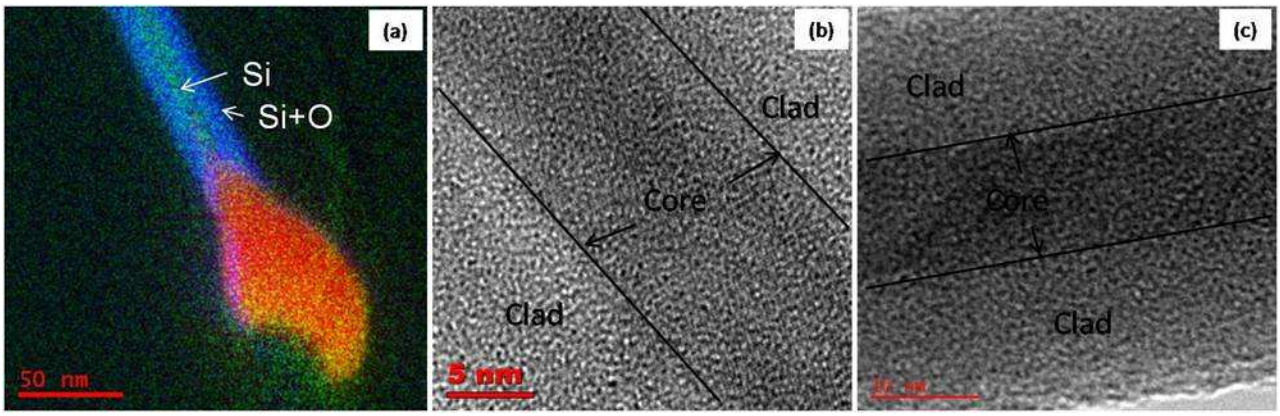

Fig.3 HRTEM analysis of SiNWs; (a) SiNW with Ni/Ti/Si substrate (sample A); Si (green), Oxygen (blue) and Ni (orange). (b) SiNWs grown on Ni/Ti/Si substrate (sample A); 12nm core diameter and 12nm oxide clad thickness and; (c) Au/Si substrate (sample B) ; 10nm core diameter and 15nm oxide clad thickness.

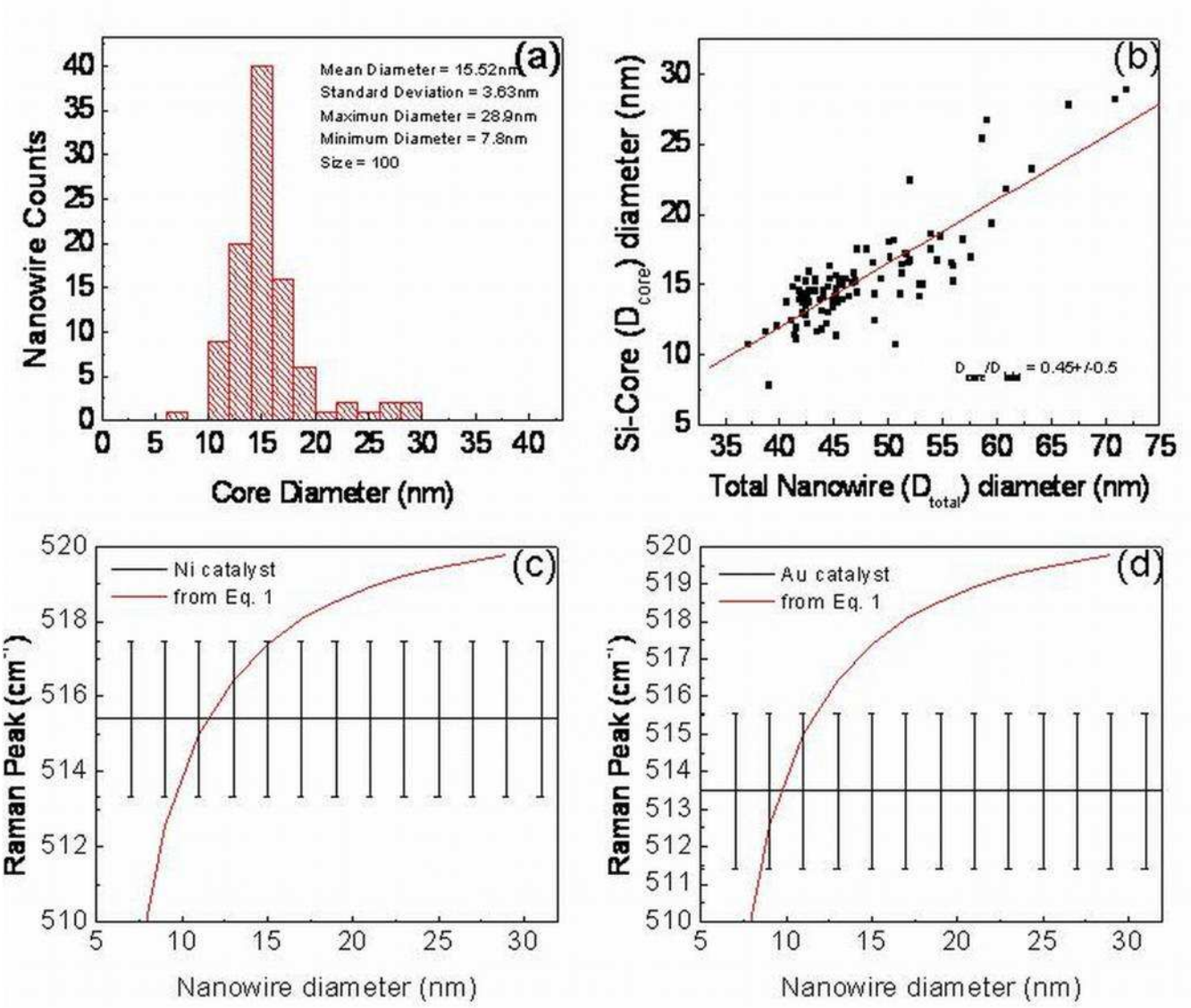

Fig.4 (a) Nanowire core diameter distribution as determined from crystalline core dimensions from HRTEM images for sample A; (b) Nanowire core diameter variation with total nanowire diameter, slope for the curve by linear fitting come 0.45±0.5nm, portray oxide clad formation during the nanowire growth itself; (c) Curve for Raman peak for sample A with Raman peak variation with nanowire diameter measured by intensity equation 1. Raman peak for sample A has ±2cm^{-1} errors which comes up with ±3.5nm diameter error; (d) Curve for Raman peak for sample B with Raman peak variation with nanowire diameter measured by intensity equation 1. Raman peak for sample A has ±2cm^{-1} error which comes up with ±2nm diameter error.

Table 1 The Raman frequency, frequency shift from the Raman frequency of c-Si, The FWHM, the coefficient of broadening (Cb) defined by FWHMSiNWs/FWHMc-Si, the asymmetric coefficient (Ca) defined by LWHM/RWHM (the left width at half maximum (LWHM) and the right width at half maximum (RWHM) from the central peak position), the diameter of the nanowires measured by TEM image and the diameter of the nanowires measured by Raman spectra.

Samples	Raman frequency (cm^{-1})	Frequency shift (cm^{-1})	FWHM (cm^{-1})	C_b	C_a	Core-diameter from TEM image (nm)	Diameter from Raman (nm)
c-Si	521.08	0	4.0831	1	1		
SiNWs-A	516.07	5.01	15.03	3.68	1.16	11	9.5
SiNWs-B	513.76	7.32	19.16	4.69	1.19	10	8